Jurnal Elektronika dan Telekomunikasi (JET), Vol. 26, No. 1, August 2026, pp. 8-15
Accredited by KEMDIKTISAINTEK, Decree No: **295/C/C3/KPT/2026**
doi: 10.55981/jet.837

Numerical Performance Analysis of Novel-Generation Materials for Mach–Zehnder Interferometer Applications

Dzulkiflih[a,*], Riski Ramadani[a], Afiyah Nikmah[a], Arum Vonie Rachmawati[a], Hanan Zaki Alhusni[b], Rohim Aminullah Firdaus[a]

[a]*Department of Physics*
Faculty of Mathematics and Natural Sciences
Universitas Negeri Surabaya
Jl. Ketintang, Ketintang, Gayungan
Surabaya, East Java 60231
[b]*Department of Physics Education*
Faculty of Mathematics and Natural Sciences
Universitas Negeri Surabaya
Jl. Ketintang, Ketintang, Gayungan
Surabaya, East Java 60231

Abstract

Advances in optical technology have driven the need for new-generation materials that are more efficient in Mach–Zehnder interferometer (MZI) structures, particularly for high-precision optical sensors and communication applications. This study aims to evaluate the optical performance of ten material configurations, namely As_2S_3, a-GST, BTO (TE), BTO (TM), c-Si, LNOI (TE), LNOI (TM), PMMA, Si_3N_4, and SU-8, in an MZI configuration using a numerical simulation approach based on the Beam Propagation Method (BPM), the Crank–Nicolson scheme, and the Padé approximation method. Simulations were conducted using MATLAB software to analyze the transverse Ey field, refractive index profiles, and optical transmission efficiency. The results indicate that materials such as BTO (TE/TM), LNOI (TE/TM), and As_2S_3 exhibit superior performance with Ey loss values ≤ 0.01, indicating excellent optical field confinement and high transmission efficiency. Meanwhile, polymer materials, such as PMMA and SU-8, exhibit poor performance with significant loss values, making them unsuitable for active waveguide functions. The novelty of this study lies in the systematic comparison of ten novel-generation material configurations under a uniform MZI simulation framework, enabling the direct evaluation of material-dependent optical confinement, Ey field loss, and transmission efficiency. These findings provide practical guidance for selecting suitable materials for next-generation MZI-based optical sensors, modulators, and integrated photonic devices.

Keywords: Mach–Zehnder interferometer, beam propagation method, new-generation materials, numerical performance analysis, refractive index.

I. INTRODUCTION

In recent decades, advances in optical technology have led to the development of various high-precision instruments that play an important role in communication, sensing, and signal processing [1-4] . One of the most prominent optical instruments is the Mach–Zehnder interferometer (MZI), a light interference-based system capable of detecting minimal changes in the refractive index or optical path length [5,6]. The MZI's simple yet flexible structure makes it a vital component in developing integrated photonic systems at the macro and nano scales [7-9] . However, the performance of the MZI is highly dependent on the characteristics of the waveguide materials used in its structure [10-12] . Conventional materials, such as silicon (Si), silica (SiO_2), and various polymers, have been widely used due to their stability and ease of fabrication [13-15] . However, the limitations of these materials—particularly in terms of miniaturization, optical transmission loss, and sensitivity to environmental changes—have driven the need for new-generation materials [16-18] . Several promising new materials have been developed to address these challenges, including amorphous germanium-antimony-tellurium (a-GST), arsenic trisulfide (As_2S_3), barium titanate oxide (BTO), crystalline silicon (c-Si), lithium niobate on insulator (LNOI), polymethyl methacrylate (PMMA), silicon nitride (Si_3N_4), and SU-8 epoxy-based photoresist [19-26]. These materials offer advantages in light transmission efficiency, adaptive environmental response, and high integration capability in nano-photonics systems. This potential makes new-generation materials an important catalyst for improving the MZI performance.

However, integrating these materials into MZI structures is not without challenges. Each material has distinct optical parameters, such as refractive index, loss coefficient, and optical conductivity, significantly influencing device performance [27-29] . Therefore, designing MZIs based on new materials requires a systematic numerical evaluation to compare how different material configurations affect optical field

* Corresponding Author.
Email: dzulkiflih@unesa.ac.id
Received: January 4, 2026 ; Revised: May 15, 2026
Accepted: May 18, 2026 ; Published: August 31, 2026

confinement, refractive index distribution, and transmission efficiency. To address these challenges, numerical simulation methods provide an effective approach for analyzing wave propagation behavior in MZI structures under consistent design conditions. One promising numerical scheme is the Crank–Nicolson scheme, which is used as a stable discretization method for solving wave propagation equations in photonic systems [30]. In this study, the Crank–Nicolson scheme is employed within the Beam Propagation Method framework as a numerical propagation tool to calculate field evolution and evaluate Ey field distribution, refractive index profiles, and optical transmission loss, not as an optimization framework [31].

Unfortunately, most existing MZI studies have focused on a single material system, a specific waveguide structure, or a particular sensing application. Previous studies have tended to focus on device-specific improvements rather than a direct comparison of multiple new-generation material configurations under identical MZI simulation conditions. As a result, there is still limited information on how different material configurations perform when evaluated using the same structural model, numerical method, and performance indicators. This creates a research gap in understanding which material configurations provide the most favorable balance between refractive index contrast, optical field confinement, and transmission efficiency for MZI applications. Therefore, this study aims to investigate the optical performance of various new-generation materials in MZI structures through a comparative numerical performance analysis based on BPM, the Crank–Nicolson scheme, and the Padé approximation method. The primary focus of this study is to investigate the characteristics of new materials to enhance the results of refractive index profiles, transverse *Ey* field distribution, and optical transmission loss. The main contribution of this study is the systematic comparison of ten material configurations within a uniform MZI model, thereby providing practical design guidance for selecting suitable materials for optical modulators, precision sensors, and next-generation integrated photonic systems. From a practical perspective, the results of this study provide guidance for selecting suitable waveguide materials for MZI-based optical modulators, refractive-index sensors, and integrated photonic devices. Compared with previous studies that mainly focused on a single material or a specific MZI structure, this work offers a broader comparative evaluation of ten material configurations under the same numerical framework, allowing more consistent assessment of material-dependent performance. This research contributes theoretically to the field of optical engineering and paves the way for the application of MZIs in high-precision sensors and next-generation optical communication systems.

II. METHODS

This study employs a numerical simulation-based approach to analyze the performance of MZI photonic structures, optical couplers, and electromagnetic field propagation in waveguides [32] . The primary method applied in this study is the Beam Propagation Method (BPM), a numerical technique used to calculate the evolution of the electric field $E(x,z)$ along the longitudinal z direction in a medium with a specific refractive index profile [33] . This method was chosen for its effectiveness in handling wave propagation in one- and two-dimensional optical structures. The basic BPM equation in this simulation approximates the Helmholtz equation and is modeled in (1) [33].

$$\frac{\partial E}{\partial z} = -\frac{j}{2k_0 n_{\text{ref}}}\left(\frac{\partial^2 E}{\partial x^2} + k_0^2\left(n(x,z)^2 - n_{\text{ref}}^2\right)E\right) \quad (1)$$

In (1), there are components such as the electric field (E), free wave number (k_0), space refractive index profile ($n(x,z)$), and reference refractive index (n_{ref}). The Crank- Nicolson scheme is used as a numerical discretization tool to solve this partial differential equation stably, as expressed in (2) [34].

$$\left(I - \frac{\Delta z}{2}A\right)E_{z+\Delta z} = \left(I + \frac{\Delta z}{2}A\right)E_z \quad (2)$$

In the Crank-Nicolson equation, component A acts as a transverse differential operator and Δz as the step length z [34]. To improve accuracy in optical structures with large propagation angles, a wide-angle approach based on Padé approximation is used. This approach replaces the propagation exponential operator with a Padé approximation form to maintain accuracy in large-angle propagation calculations by mathematically modelling it in (3) [35].

$$e^{j\Delta z\cdot\sqrt{k_0^2 n^2 - \nabla_\perp^2}} \approx Padé\ Approximation \quad (3)$$

After the electric field was obtained from the BPM model, an optical mode analysis was performed to evaluate the supermodes formed in the directional coupler structure. Two supermodels were identified: symmetric and anti-symmetric modes. The difference in effective index between the two (Δn_{eff}) was used to calculate the coupling length (L_c), determining the distance energy can be transferred entirely from one waveguide to another. The coupling length was calculated using (4) [36].

$$L_c = \frac{\lambda}{2\cdot|\Delta n_{eff}|} = \frac{\lambda}{2\cdot|n_{eff,even} - n_{eff,odd}|} \quad (4)$$

From the value L_c in (4), the coupling coefficient (κ) is obtained, which indicates the strength of the interaction between waveguides, and the power transferred in the tap coupler along the length (L_{cp}) is also calculated [36]. Furthermore, the MZI structure has a phase difference between the two MZI arms, which is crucial for optical modulation. This difference arises due to variations in the refractive index in one of the arms, which can be caused by heating, pressure, or external electric fields. The phase difference is calculated using (5) [37].

$$\Delta\Phi = \frac{2\pi}{\lambda} \cdot |n_{eff,1} - n_{eff,2}| \cdot L_{MZI} \quad (5)$$

In (5), $n_{\text{eff},1}$ and $n_{\text{eff},2}$ are the effective indices of each arm, and L_{MZI} is the length of the MZI arm [37]. To evaluate the modulator response, the target phase difference was set to produce destructive interference, so that the transmitted output power could be minimized. To achieve this condition, interpolation is performed on the relationship between the change in refractive index (Δn)and the change in effective index (Δn), which is obtained from the simulation results. Using this data, the value Δn causing is $\Delta\Phi = \pi$ determined so that the modulator is in the maximum off condition [38]. This relationship can be written inversely in (6) [38].

$$\Delta n = \frac{\lambda}{2L_{\text{MZI}}} \quad (6)$$

All mathematical models from (1) to (6) were implemented into MATLAB simulations, and the programming flow design was visualized in Fig. 1. Based on the simulation modelling results shown in Fig. 1, a visualization of the refractive index profile, electric field magnitude Ey, electric field phase Ey, changes in the waveguide refractive index, and power loss occurring due to the application of each new material in the simulation structure was obtained. The types of materials used in the simulation model in Figure 1 are presented in detail in Table 1.

The materials in Table 1 were selected for this MZI simulation based on their optical characteristics and applicability in integrated photonic systems. As_2S_3 was chosen for its high refractive index and good nonlinear response. BTO (TE and TM) was used for its strong electro-optic properties, ideal for active modulators. c-Si serves as an industry standard with CMOS compatibility. LNOI (TE and TM) was chosen for its ability to enable fast modulation. PMMA and SU-8 represent flexible polymer materials with low to moderate refractive indices. Meanwhile, Si_3N_4 was selected due to its low loss and high stability. These materials represent various materials to evaluate MZI performance regarding the transverse *Ey* field, refractive index profiles, and optical transmission efficiency (power loss).

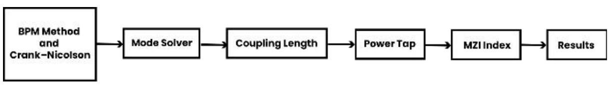

Figure 1. Workflow of the numerical MZI simulation based on BPM, the Crank–Nicolson scheme, and the Padé approximation.

TABLE 1
THE REFRACTIVE INDEX PARAMETERS OF THE EVALUATED MATERIAL CONFIGURATIONS

Material	Core	Substrate	Reference
As_2S_3	1.444	2.41	[19]
a-**GST**	1.444	4.037	[20]
BTO (TE)	1.444	2.383	[21]
BTO (TM)	1.444	2.444	[21]
c-SI	1.444	3.48	[22]
LNOI (TM)	1.444	2.211	[26]
LNOI (TE)	1.444	2.138	[26]
PMMA	1.0	1.481	[23]
Si_3N_4	1.444	2.0	[24]
SU-8	1.444	1.575	[25]

III. RESULTS AND DISCUSSION

In a MZI system simulation, selecting the waveguide material is the primary determinant in determining how the transverse electric field energy (Ey) can be maintained from the input point to the output. The MZI operates based on the principle of interference between two light beams that experience phase differences due to differences in their paths or the properties of the materials they pass through. Therefore, the stability and efficiency of the electromagnetic field transmission within the waveguide structure are critical. Based on Table 2, each material's performance can be analyzed based on the Ey field loss values obtained from numerical simulations. The results show a clear quantitative relationship between the refractive index contrast, Ey field confinement, and optical transmission performance. Material configurations with stable refractive index profiles and stronger mode confinement, such as BTO, LNOI, and As_2S_3, exhibit the lowest Ey loss values of 0.01, whereas polymer-based configurations with weak confinement, such as PMMA and SU-8, show much higher losses of 0.11 and 0.89. The quantitative results in Table 2 show that material configurations with stronger optical confinement generally produce lower Ey field loss. The best-performing configurations, namely LNOI (TE/TM), BTO (TE/TM), and As_2S_3, maintain an output Ey value of 0.98 from an input value of 0.99, corresponding to a loss of only 0.01. This indicates that approximately 98.99% of the input field amplitude is retained after propagation. Si_3N_4 retains 0.97 from 0.99, corresponding to a loss of 0.02, while c-Si and a-GST retain 0.96–0.97 with a loss of 0.03. In contrast, PMMA retains only 0.73 from 0.84, and SU-8 decreases sharply from 0.92 to 0.03, indicating severe field attenuation. These quantitative differences confirm that the optical performance is strongly affected by the ability of each material configuration to confine the Ey field inside the waveguide region.

Based on Table 2, c-Si material shows a loss of 0.03 with an input of 0.99 and an output of 0.96.

TABLE 2
INPUT, OUTPUT, AND LOSS VALUES OF THE TRANSVERSE ELECTRIC FIELD COMPONENT EY FOR EACH MATERIAL CONFIGURATION

Material	Input	Output	Loss
c-Si	0.99	0.96	0.03
Si_3N_4	0.99	0.97	0.02
LNOI (TE)	0.99	0.98	0.01
LNOI (TM)	0.99	0.98	0.01
PMMA	0.84	0.73	0.11
SU-8	0.92	0.03	0.89
a-GST	1.0	0.97	0.03
BTO (TE)	0.99	0.98	0.01
BTO (TM)	0.99	0.98	0.01
As_2S_3	0.99	0.98	0.01

Although it is still considered to be within the high-efficiency threshold, this loss indicates that the *Ey* field energy is degraded as it propagates through this material [22] . The relatively high refractive index of c-Si provides strong optical confinement; however, excessive index contrast may also increase sensitivity to mode mismatch and scattering at waveguide transitions, leading to a measurable Ey loss of 0.03. However, since c-Si is compatible with CMOS technology and has proven stable across various wavelengths, this material remains a leading candidate for integrated MZIs, particularly in silicon photonics systems [39] . Additionally, Si_3N_4 demonstrates superior performance with a loss of only 0.02. Compared with c-Si, Si_3N_4 provides a more moderate refractive index contrast, which can reduce field leakage and transition-related attenuation while still maintaining sufficient confinement. This explains why the Ey loss decreases from 0.03 in c-Si to 0.02 in Si_3N_4. Si_3N_4 is also known for its low propagation loss in the near-infrared (NIR) wavelength range, making it suitable for high-precision sensor-based MZIs and optical communication applications.

One of the most notable results comes from LNOI in both TE and TM modes, with a loss of only 0.01. This material is known for its excellent electro-optic and piezoelectric properties and a relatively high refractive index without causing significant parasitic reflections [26] . Quantitatively, both LNOI modes maintain an output Ey value of 0.98 from an input of 0.99, showing that only a very small portion of the transverse field amplitude is attenuated during propagation. This low loss indicates that the refractive index profile of LNOI provides effective mode confinement while minimizing field leakage outside the waveguide core. Its stability under temperature and modulation speed makes LNOI highly suitable for MZIs, particularly in active optical systems such as modulators and electric field sensors. Similarly, BTO in both TE and TM modes also exhibits low loss (0.01). BTO is known for its high electro-optic coefficient and ability to adapt to high-pressure or high-electric-field environments [40]. The similar loss values obtained for BTO (TE) and BTO (TM) indicate that both polarization configurations can preserve the Ey field efficiently under the simulated MZI structure. Therefore, the quantitative relationship between refractive index distribution and Ey loss suggests that BTO and LNOI are more suitable for active MZI devices requiring stable field confinement and high transmission efficiency. This makes BTO a candidate for MZI applications in precise quantitative sensing fields, such as optical biosensors or electro-optic interferometry.

On the other hand, a-GST, a phase-change material commonly used in optical memory, exhibits a loss of 0.03. This value is comparable to c-Si and remains within the medium efficiency range. This material has the potential for use in MZI, requiring structural adaptability, such as an optical switch, as it can be switched between amorphous and crystalline states thermally or optically [41]. However, its use in passive MZI still requires solutions for heat dissipation.

In contrast, PMMA and SU-8, photosensitive polymers for coatings and microstructures, exhibit the worst performance. PMMA exhibited a loss of 0.11, while SU-8 was extremely high at 0.89. The quantitative difference between input and output values indicates that PMMA retains only about 86.90% of its initial Ey amplitude, while SU-8 retains only about 3.26%. This severe reduction is associated with weak optical confinement caused by low refractive index contrast between the polymer core and surrounding medium. As a result, a large portion of the optical field spreads outside the intended guiding region, increasing attenuation and reducing transmission efficiency. SU-8 even produced an output of only 0.03 from an input of 0.92, indicating that this material is unsuitable for MZI waveguides. However, it can still be used as a protective layer or passive microstructure.

Meanwhile, As_2S_3 demonstrates excellent performance with a loss of 0.01. As_2S_3 is one of the chalcogenide glass materials with a high refractive index, a wide transparency range in the infrared spectrum, and high optical nonlinearity [19] . This makes it highly promising for infrared sensing-based MZI applications or ultra-fast optical processing. Further analysis of the refractive index profiles for each material in the MZI simulation is shown in Figure 2.

Figure 2 shows the results of numerical simulations of the selection of waveguide materials that significantly affect the efficiency of transverse electric field (*Ey*) transmission in a MZI structure. Based on the top-view visualization of the refractive index profile of each material, it is evident that the contrast between the waveguide core and the surrounding medium plays a crucial role in determining the strength of light confinement. Materials such as a-GST (amorphous $Ge_2Sb_2Te_5$) and c-Si (crystalline silicon) exhibit structures with very high refractive index contrasts, ranging from 3.4 to over 4.2. This contrast indicates good ability to control the optical field, as evidenced by the relatively low output loss of the *Ey* field, which is 0.03. Meanwhile, materials such as As_2S_3, BTO (TE/TM), and LNOI (TE/TM) exhibit structures with symmetrical and stable refractive index distributions in the range of 1.5-2.4. This distribution facilitates light propagation with optimal mode confinement and minimal scattering, resulting in a very low transmission loss of only 0.01. Notably, BTO and LNOI exhibit high electro-optic properties, making them highly relevant for application in active MZIs such as light modulators, pressure sensors, or high-speed tuning interferometers. The refractive index distribution in simulations also shows a consistent core width of the waveguide, ensuring stability of transverse modes during propagation.

In contrast, poor performance is demonstrated by polymer materials such as PMMA and SU-8, which exhibit relatively flat refractive index distributions with low contrast below 1.56. As a result, most of the *Ey* field energy cannot be effectively guided, leading to very high losses of 0.11 and 0.89, respectively. SU-8, in particular, can only retain 3% of the input field, indicating that this material is highly unsuitable as a waveguide core in precision interferometric systems.

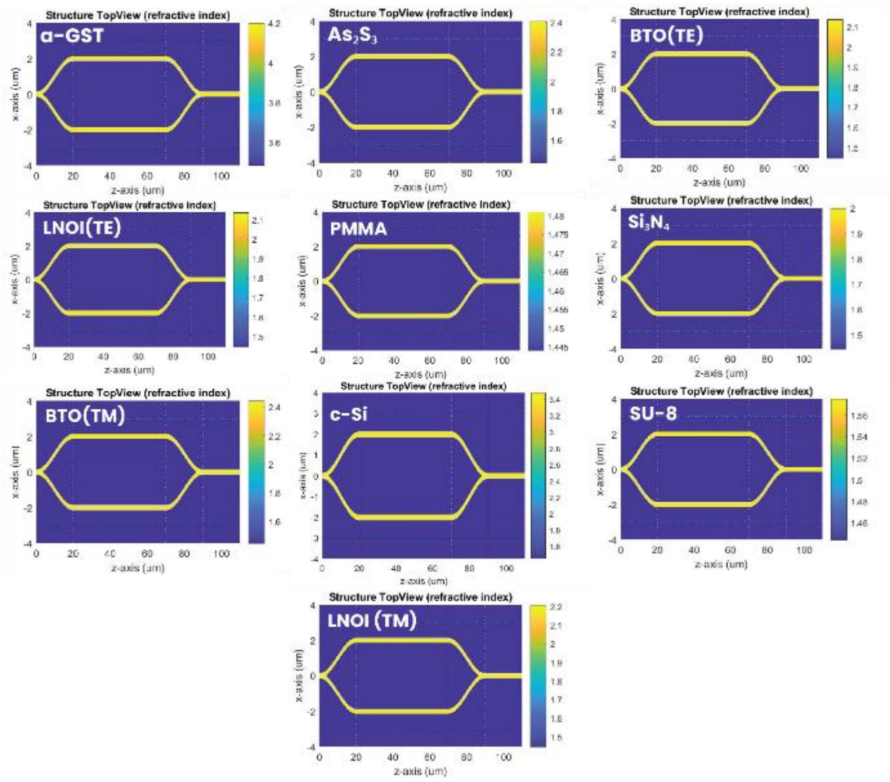

Figure 2. The refractive index profiles of the evaluated material configurations in the MZI structure.

Although both materials are commonly used in lithography or microstructure fabrication, their application in MZI optical cores hinders device performance [23] . Si_3N_4 (silicon nitride), on the other hand, occupies an intermediate position in MZI performance, with adequate refractive index contrast (1.45–2.0) and a clean distribution structure. This results in a loss of only 0.02, making it an ideal candidate for CMOS-based MZI applications, as it is compatible with standard fabrication processes and exhibits high stability against temperature and wavelength fluctuations. The refractive index profile in Figure 2 explains the loss trend observed in Table 2. Materials with balanced refractive index contrast, such as BTO, LNOI, As_2S_3, and Si_3N_4, support stronger mode confinement and therefore show lower Ey loss values between 0.01 and 0.02. In contrast, polymer materials with weaker refractive index contrast, particularly PMMA and SU-8, show poor confinement and higher loss values of 0.11 and 0.89. This relationship demonstrates how the refractive index parameter directly affects field localization, propagation stability, and transmission efficiency in the MZI structure. Further analysis of the intensity of the transverse electric field during light propagation through the MZI structure is presented in Figure 3.

Figure 3 shows the simulation results of the propagation of the transverse field |Ey| in the MZI structure, revealing significant differences in the confinement and energy attenuation patterns of the field based on the characteristics of each waveguide material. The visualization in Figure 3 illustrates the distribution of *Ey* field intensity along the z-axis (propagation direction) and the x-axis (transverse direction) within a dynamic range of 0 to -30 dB. Yellow to red colors indicate high intensity (approaching 0 dB), while blue gradients indicate energy attenuation due to optical loss and diffraction. From Fig. 3, materials such as a-GST, As_2S_3, BTO (TE and TM), and LNOI (TE) exhibit highly stable and concentrated Ey field transmission performance within the waveguide boundaries. A consistent yellow-to-green color distribution along the main MZI path characterizes this. No significant intensity spread outside the waveguide boundaries is observed in this structure, indicating effective optical mode confinement and low loss. This feature aligns with the low numerical loss values (≤0.03) listed in Table 2. Specifically, As_2S_3 and BTO demonstrate superiority as passive and electro-optic material candidates with highly efficient propagation capabilities for wave propagation. Meanwhile, Si_3N_4 and c-Si also exhibit satisfactory performance, with well-maintained propagation paths and relatively small field attenuation outside the waveguide core. The green color on the core boundary indicates that a small portion of the field energy leaks but remains within acceptable limits, particularly for MZI applications that do not require extreme sensitivity. The stability of Si_3N_4 in CMOS fabrication and its compatibility with telecommunication wavelengths make it relevant for integrated MZI designs.

In contrast, LNOI (TM) exhibits fluctuations in field intensity along the propagation path with the appearance of unstable transverse interference patterns marked by color variations within the waveguide boundary. This indicates the presence of mode coupling or birefringence effects that affect propagation stability in the TM mode. This phenomenon must be considered in LNOI-based MZI designs for sensor or modulator applications to achieve optimal polarization orientation. PMMA and SU-8, which are optical polymers, exhibit abysmal performance in Ey field propagation.

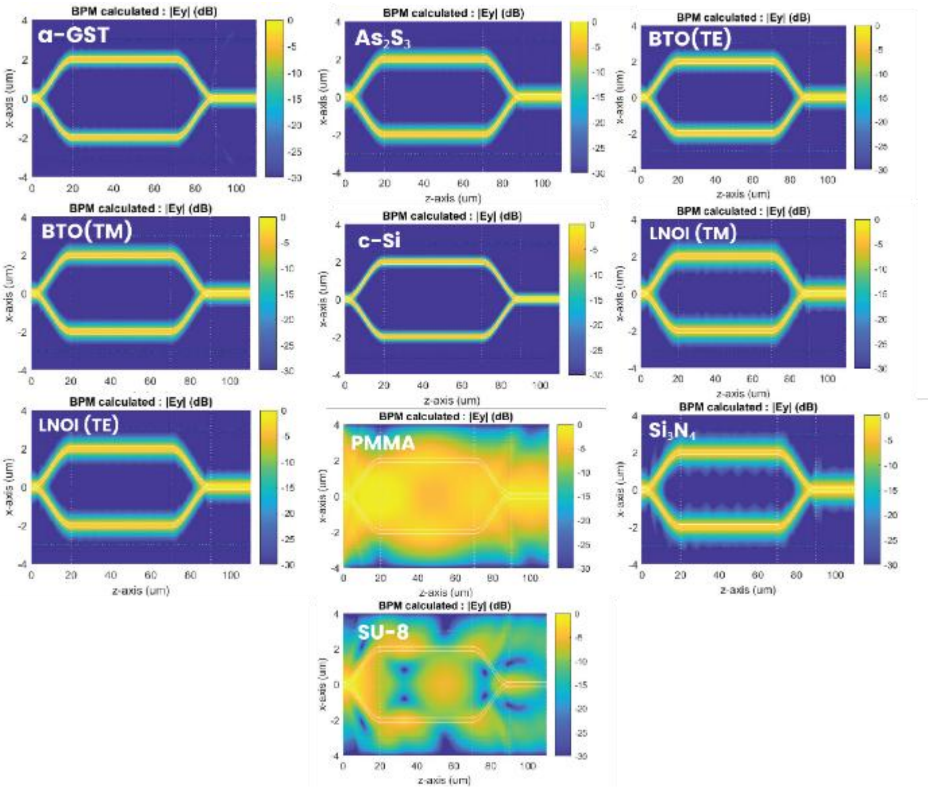

Figure 3. Distribution of transverse Ey field intensity for each material configuration in the MZI structure.

Visualization of the *Ey* field in PMMA shows widespread dispersion, with yellow dominating the area outside the waveguide core. This indicates that the field is not concentrated and experiences significant attenuation even from the onset of propagation. SU-8 is even more extreme, with spot loss and random interference appearing, indicating that the *Ey* field energy cannot sustain itself within the structure. Both materials have low refractive indices and minimal refractive index contrast with their surroundings, resulting in weak optical confinement. Therefore, PMMA and SU-8 are deemed unsuitable as waveguide cores for optical interferometry applications, although they remain relevant as coating materials or masks in lithography processes [23] . The overall results of this study are presented in Table 3. The field distribution in Figure 3 further confirms the quantitative loss data. Materials with low loss values show a concentrated Ey distribution along the propagation path, whereas materials with high loss values show broader field spreading and irregular intensity patterns. This means that the numerical loss values are not only output indicators but also directly reflect the physical propagation behavior inside the MZI structure. Therefore, the combination of Table 2, Figure 2, and Figure 3 demonstrates a consistent parameter-performance relationship: higher confinement quality and more suitable refractive index contrast lead to lower Ey loss and better optical transmission efficiency.

TABLE 3
COMPARISON OF THIS STUDY WITH PREVIOUS MZI-RELATED MATERIAL AND METHOD STUDIES

Reference	Research Focus	Material	Method
[42]	Strip-loaded MZI for sensing	TiO_2 – nLOF polymer	3D-FDTD
[43]	Improved gas phase detection	Silicon	Experiment + phase unwrap
[44]	MZI fiber for seawater sensing	Core-offset fiber	Experiment
[45]	Photochromic film-based quantum MZI	Chromene	Simulation and experiments
[46]	Optical memory MZI	GeSe–SOI	BPM + Eigenmode analysis
This work	Comparative numerical analysis of ten MZI material configurations	AS_2S_3, BTO (TE), BTO (TM), c-SI, LNOI (TM), LNOI (TE), PMMA, Si_3N_4, a-GST, and SU-8	BPM + Crank–Nicolson scheme + Padé approximation

Table 3 compares this study with recent research trends in MZI development. Several international publications have attempted to improve MZI performance through various approaches, including specific sensor structures, phase correction methods, fiber-based configurations, photochromic films, and phase-change materials. However, most previous studies focused on a single material system, a specific sensing target, or a particular device configuration. In contrast, this study provides a broader practical contribution by comparing ten material configurations under the same MZI simulation framework, enabling direct evaluation of material-dependent differences in optical confinement, Ey field loss, and transmission efficiency. This comparison can support material selection at the early design stage of MZI-based sensors, modulators, and integrated photonic devices. No systematic study has tested and compared the performance of various new-generation material configurations in a uniform MZI structural model using the same numerical simulation framework. This marks a research gap in the literature, particularly regarding the integrative aspect between material physical characteristics and numerical design strategies. This research aims to bridge this gap by comparing the performance of ten new-generation material configurations, As_2S_3, BTO (TE), BTO (TM), c-Si, LNOI (TM), LNOI (TE), PMMA, Si_3N_4, a-GST, and SU-8, in numerically simulated MZI structures. The Beam Propagation Method combined with the Crank–Nicolson scheme and the Padé approximation approach facilitates accurate electromagnetic field propagation calculations, even at large propagation angles. The main advantage of this research lies in applying the BPM combined with the Crank–Nicolson scheme and Padé approximation to evaluate electromagnetic field propagation consistently across different material configurations, enabling direct comparison of optical confinement, Ey field loss, and transmission efficiency. Simulation results show that BTO (TE/TM), LNOI (TE/TM), and As_2S_3 materials exhibit the best performance with Ey loss values ≤ 0.01, making them strong candidates for MZI implementation in optical modulators, pressure sensors, and high-precision interference-based detection applications. On the other hand, materials such as PMMA and SU-8 exhibit significant loss, indicating that their optical characteristics are unsuitable for use as waveguide cores in active MZI systems. However, they remain relevant for passive applications or as protective layers.

IV. CONCLUSION

In this study the performance of ten material configurations in MZI structures was investigated through numerical simulations using the beam propagation method combined with the Crank–Nicolson scheme and the Padé approximation. The simulation results showed that material selection significantly affects the transmission efficiency and the magnitude of the Ey transverse electric field loss. Materials such as As_2S_3, BTO (TE and TM), and LNOI (TE and TM) exhibit the best performance with very low loss values (≤ 0.01), indicating optimal light confinement and high compatibility for MZI applications in optical modulators and precision sensors. Si_3N_4 and c-Si also provide good performance with loss values of 0.02 and 0.03, respectively, and offer advantages in CMOS compatibility and wavelength stability. In contrast, polymer materials such as PMMA and SU-8 exhibit high loss values of up to 0.11 and 0.89, making them unsuitable as waveguide cores. However, they remain relevant for structural or coating applications. The strength of this research lies in integrating material physical characteristics with a comparative numerical simulation framework based on BPM, the Crank–Nicolson scheme, and the Padé approximation, which enables consistent evaluation of material-dependent optical performance in MZI structures. These findings provide practical guidance for selecting suitable material configurations for MZI-based optical modulators, refractive-index sensors, and integrated photonic devices. However, because this study is limited to numerical analysis under fixed structural parameters, future research should include experimental validation, wavelength-dependent investigation, and waveguide geometry refinement to further confirm the applicability of the best-performing materials.

DECLARATIONS

Conflict of Interest

The authors declare that there is no conflict of interest regarding this manuscript or the published research results, including any financial aspects related to the conduct of the study, the acquisition and application of its outcomes, and any non-financial personal relationships.

CRediT Authorship Contribution

Riski Ramadani: Conceptualization, Methodology, Software, and Original Draft Writing; Afiyah Nikmah: Data Curation, Validation, and Original Draft Writing; Arum Vonie Rachmawati: Investigation, Visualization, Review and Editing; Hanan Zaki Alhusni: Investigation, Validation, Review and Editing; Rohim Aminullah Firdaus: Resources, Visualization, Review and Editing; and Dzulkiflih: Supervision, Project Administration, Funding Acquisition, Review and Editing.

Funding

This research received no specific grant from any funding agency in the public, commercial, or not-for-profit sectors.

REFERENCES

[1] H. Wang, J.-K. Guo, H. Mo, X. Zhou, and Y. Han, “Fiber Optic Sensing Technology and Vision Sensing Technology for Structural Health Monitoring,” *Sensors*, vol. 23, no. 9, p. 4334, Apr. 2023, doi: 10.3390/s23094334.

[2] S. Wang, R. Ma, F. Cao, L. Luo, and X. Li, “A review: High-precision angle measurement technologies,” *Sensors*, vol. 24, no. 6, p. 1755, Mar. 2024, doi: 10.3390/s24061755.

[3] M. F. S. Ferreira *et al.*, “Roadmap on optical sensors,” *J. Opt.*, vol. 19, no. 8, p. 083001, Aug. 2017, doi: 10.1088/2040-8986/aa7419.

[4] S. N. Khonina, N. L. Kazanskiy, R. V. Skidanov, and M. A. Butt, “Advancements and Applications of Diffractive Optical Elements in Contemporary Optics: A Comprehensive Overview,” *Adv. Mater. Technol.*, vol. 10, no. 4, Feb. 2025, doi: 10.1002/admt.202401028.

[5] Z. Cao, M. Shao, Y. Yuan, X. Ma, Y. Yu, and X. Qiao, “In-fiber Mach-Zehnder interferometer for wearable respiration measurement,” *Sensors and Actuators A: Physical*, vol. 364, p. 114806, Dec. 2023, doi: 10.1016/j.sna.2023.114806.

[6] J. Wang, Y. Zhang, and X. Gu, “A Partial Discharge Detection Approach in Distribution Cabinets Using a Mach–Zehnder Interferometer,” *Sensors*, vol. 25, no. 7, p. 2265, Apr. 2025, doi: 10.3390/s25072265.

[7] Y. Xu, B. Xiong, W. Ma, and Y. Liu, “Software-defined nanophotonic devices and systems empowered by machine learning,” *Prog. Quantum Electron.*, vol. 89, p. 100469, May 2023, doi: 10.1016/j.pquantelec.2023.100469.

[8] S. N. Khonina, G. S. Voronkov, E. P. Grakhova, N. L. Kazanskiy, R. V. Kutluyarov, and M. A. Butt, “Polymer Waveguide-Based Optical Sensors—Interest in Bio, Gas, Temperature, and Mechanical Sensing Applications,” *Coatings*, vol. 13, no. 3, p. 549, Mar. 2023, doi: 10.3390/coatings13030549.

[9] A. H. Atabaki *et al.*, “Integrating photonics with silicon nanoelectronics for the next generation of systems on a chip,” *Nature*, vol. 556, no. 7701, pp. 349–354, Apr. 2018, doi: 10.1038/s41586-018-0028-z.

[10] C. S. Rizal and B. Niraula, "Compact Si-based asymmetric MZI waveguide on SOI as a thermo-optical switch," *Opt. Commun.*, vol. 410, pp. 947–955, Mar. 2018, doi: 10.1016/j.optcom.2017.10.007.

[11] Y. Su, Y. Zhang, C. Qiu, X. Guo, and L. Sun, "Silicon Photonic Platform for Passive Waveguide Devices: Materials, Fabrication, and Applications," *Adv. Mater. Technol.*, vol. 5, no. 8, Aug. 2020, doi: 10.1002/admt.201901153.

[12] R. Halir *et al.*, "Waveguide sub-wavelength structures: a review of principles and applications," *Laser. Photon. Rev.*, vol. 9, no. 1, pp. 25–49, Jan. 2015, doi: 10.1002/lpor.201400083.

[13] M. Sajjad, "Recent Advances in SiO2 Based Composite Electrodes for Supercapacitor Applications," *J. Inorg. Organomet. Polym. Mater.*, vol. 31, no. 8, pp. 3221–3239, Aug. 2021, doi: 10.1007/s10904-021-01899-1.

[14] R. Ciriminna, A. Fidalgo, V. Pandarus, F. Béland, L. M. Ilharco, and M. Pagliaro, "The Sol–Gel Route to Advanced Silica-Based Materials and Recent Applications," *Chem. Rev.*, vol. 113, no. 8, pp. 6592–6620, Aug. 2013, doi: 10.1021/cr300399c.

[15] H. Li *et al.*, "Recent research progress and advanced applications of silica/polymer nanocomposites," *Nanotechnol. Rev.*, vol. 11, no. 1, pp. 2928–2964, Oct. 2022, doi: 10.1515/ntrev-2022-0484.

[16] G. Li, T. Li, Y. Liu, and Y. Zheng, "A new Mach–Zehnder interference temperature measuring sensor based on silica-based chip," *Sci. Rep.*, vol. 14, no. 1, p. 8657, Apr. 2024, doi: 10.1038/s41598-024-59447-z.

[17] X. Liu, Y. Gu, T. Mi, X. Wang, and X. Zhang, "Dip-Coating Approach to Fabricate Durable PDMS/STA/SiO2 Superhydrophobic Polyester Fabrics," *Coatings*, vol. 11, no. 3, p. 326, Mar. 2021, doi: 10.3390/coatings11030326.

[18] C. Zhao *et al.*, "Recent advances in fiber optic sensors for respiratory monitoring," *Optical Fiber Technology*, vol. 72, p. 103000, Sep. 2022, doi: 10.1016/j.yofte.2022.103000.

[19] J. M. Laniel, N. Hô, R. Vallée, and A. Villeneuve, "Nonlinear-refractive-index measurement in As2S3 channel waveguides by asymmetric self-phase modulation," *J. Opt. Soc. Am. B*, vol. 22, no. 2, p. 437, Feb. 2005, doi: 10.1364/JOSAB.22.000437.

[20] X. Ji *et al.*, "Ultrasensitive SPR Sensor Using PDMS-Filled Side-Polished Hollow-Core Fiber," *IEEE Sensors J.*, vol. 24, no. 24, pp. 40866–40872, Dec. 2024, doi: 10.1109/JSEN.2024.3477939.

[21] M. Tao *et al.*, "Towards high quality transferred barium titanate ferroelectric hybrid integrated modulator on silicon," *Light: Advanced Manufacturing*, vol. 5, no. 4, p. 1, 2024, doi: 10.37188/lam.2024.031.

[22] J. Song, S. Ghosh, N. Dhingra, H. Zhang, L. Zhou, and B. M. A. Rahman, "Feasibility study of a Ge 2 Sb 2 Te 5 -clad silicon waveguide as a non-volatile optical on-off switch," *OSA. Contin.*, vol. 2, no. 1, p. 49, Jan. 2019, doi: 10.1364/OSAC.2.000049.

[23] D. Paradita, I. Yulianti, and M. Suhantoro, "Fabrication and Characterization of Core Offset Waveguide Optical Sensor for Refractive Index Measurement," *Indonesian J. Appl. Phys.*, vol. 12, no. 2, p. 163, Nov. 2022, doi: 10.13057/ijap.v12i2.51833.

[24] V. Vitali, C. Lacava, T. D. Bucio, F. Y. Gardes, and P. Petropoulos, "Bi-Layer Grating Couplers for Hybrid Si_xN_y-Si_3N_4 Photonics with Sub- Decibel Coupling Efficiency," in *2023 Conference on Lasers and Electro-Optics Europe & European Quantum Electronics Conference (CLEO/Europe-EQEC)*, IEEE, Jun. 2023, pp. 1–1. doi: 10.1109/CLEO/Europe-EQEC57999.2023.10232562.

[25] A. Piruska, A. A. S. Bhagat, K. Zhou, E. T. K. Peterson, I. Papautsky, and C. J. Seliskar, "Characterization of SU-8 optical multimode waveguides for integrated optics and sensing on microchip devices," In *Microfluidics, BioMEMS, and Medical Microsystems IV,* vol. 6112, pp. 54-62 Jan. 2006, doi: 10.1117/12.655667.

[26] Y. Wang, Z. Chen, and H. Hu, "Analysis of Waveguides on Lithium Niobate Thin Films," *Crystals (Basel)*, vol. 8, no. 5, p. 191, Apr. 2018, doi: 10.3390/cryst8050191.

[27] J. Wu *et al.*, "Two-Dimensional Materials for Integrated Photonics: Recent Advances and Future Challenges," *Small Sci.*, vol. 1, no. 4, Apr. 2021, doi: 10.1002/smsc.202000053.

[28] C. Peng *et al.*, "Optical Waveguide Refractive Index Sensor for Biochemical Sensing," *Applied Sciences*, vol. 13, no. 6, p. 3829, Mar. 2023, doi: 10.3390/app13063829.

[29] S. Altaleb *et al.*, "Design and optimization of a high-speed ITO-plasmon-based asymmetric Mach-Zehnder interferometer modulator," in *Physics and Simulation of Optoelectronic Devices XXXII*, vol. XXXII, SPIE, Mar. 2024, p. 13. doi: 10.1117/12.3003419.

[30] A. A. Alanazi, S. Z. Alamri, S. Shafie, and S. Mohd Puzi, "Crank-Nicolson Scheme for Solving the Modified Nonlinear Schrodinger Equation," *Int. J. Numer. Methods. Heat Fluid Flow*, vol. 31, no. 8, pp. 2789–2817, Aug. 2021, doi: 10.1108/HFF-10-2020-0677.

[31] Z. Jakšić, S. Devi, O. Jakšić, and K. Guha, "A Comprehensive Review of Bio-Inspired Optimization Algorithms Including Applications in Microelectronics and Nanophotonics," *Biomimetics*, vol. 8, no. 3, p. 278, Jun. 2023, doi: 10.3390/biomimetics8030278.

[32] Y. Chen and Q. Qiu, "A novel microring resonator based on multi-Mach–Zehnder interferometers," *Opt. Commun.*, vol. 483, p. 126643, Mar. 2021, doi: 10.1016/j.optcom.2020.126643.

[33] K. Okamoto, "Beam propagation method," in *Fundamentals of Optical Waveguides*, Elsevier, 2006, pp. 329–397. doi: 10.1016/B978-012525096-2/50008-8.

[34] D. A. Ketzaki, I. T. Rekanos, T. I. Kosmanis, and T. V. Yioultsis, "Beam Propagation Method Based on the Iterated Crank–Nicolson Scheme for Solving Large-Scale Wave Propagation Problems," *IEEE Trans. Magn.*, vol. 51, no. 3, pp. 1–4, Mar. 2015, doi: 10.1109/TMAG.2014.2354979.

[35] M. C. Lytaev, "On application of the finite-difference Padé approximation of the pseudo-differential parabolic equation to the tropospheric radio wave propagation problem," *Numerical Methods and Programming (Vychislitel'nye Metody i Programmirovanie)*, no. 4, pp. 405–419, Oct. 2020, doi: 10.26089/NumMet.v21r433.

[36] R. Cheng, W. Wang, R. Sun, A. Li, and Y. Liang, "Broadband, compact and reflection-less silicon polarizer and polarization beam splitter using chirped anti-symmetric multimode nanobeams," *Opt. Express*, vol. 31, no. 12, p. 19347, Jun. 2023, doi: 10.1364/OE.487155.

[37] Y. Zhao *et al.*, "Study of resonant mode coupling in the transverse-mode-conversion based resonator with an anti-symmetric nanobeam Bragg reflector," *Opt. Express*, vol. 31, no. 4, p. 6577, Feb. 2023, doi: 10.1364/OE.481946.

[38] C. Chen *et al.*, "Design and optimization of diamond mid-infrared phase shifter," *Functional Diamond*, vol. 1, no. 1, pp. 117–124, Jan. 2021, doi: 10.1080/26941112.2020.1869485.

[39] A. Trita, A. Thomas, and A. Rickman, "CMOS compatible athermal silicon photonic filters based on hydrogenated amorphous silicon," *Opt. Express*, vol. 30, no. 11, p. 19311, May 2022, doi: 10.1364/OE.446998.

[40] D. Chelladurai *et al.*, "Barium titanate and lithium niobate permittivity and Pockels coefficients from megahertz to sub-terahertz frequencies," *Nat. Mater*, vol. 24, no. 6, pp. 868–875, Jun. 2025, doi: 10.1038/s41563-025-02158-1.

[41] A. Bose and R. Chakraborty, "Thermally tuned on-chip optical memory," *Phys. Scr.*, vol. 99, no. 9, p. 095538, Sep. 2024, doi: 10.1088/1402-4896/ad6e36.

[42] I. Doughan, K. Oyemakinwa, O. Ovaskainen, and M. Roussey, "Strip-loaded Mach–Zehnder interferometer for absolute refractive index sensing," *Sci. Rep.*, vol. 14, no. 1, p. 3064, Feb. 2024, doi: 10.1038/s41598-024-53326-3.

[43] L. Laplatine, S. Messaoudene, N. Gaignebet, C. Herrier, and T. Livache, "Correction of 2π Phase Jumps for Silicon Photonic Sensors Based on Mach Zehnder Interferometers with Application in Gas and Biosensing," *Sensors*, vol. 24, no. 5, p. 1712, Mar. 2024, doi: 10.3390/s24051712.

[44] J. Zhou *et al.*, "The Highly Sensitive Refractive Index Sensing of Seawater Based on a Large Lateral Offset Mach–Zehnder Interferometer," *Sensors*, vol. 24, no. 12, p. 3887, Jun. 2024, doi: 10.3390/s24123887.

[45] F. Scotognella, "Quantum computation with photochromic films in a Mach–Zehnder interferometer," *Front. Nanotechnol.*, vol. 6, Nov. 2024, doi: 10.3389/fnano.2024.1422573.

[46] R. Dwivedi, F. Pavanello, and R. Orobtchouk, "An ultra-low-loss compact phase-change material-based hybrid-mode interferometer for photonic memories," *APL Mater.*, vol. 13, no. 4, Apr. 2025, doi: 10.1063/5.0245618.